

A Definitive Example of a Geometric “Entatic State” Effect: Electron-Transfer Kinetics for a Copper(II/I) Complex Involving A Quinquedentate Macrocyclic Trithiaether–Bipyridine Ligand

Gezahegn Chaka,^{1a} Jason L. Sonnenberg,^{1a} H. Bernhard Schlegel,^{1a}
Mary Jane Heeg,^{1a} Gregory Jaeger,^{1b} Timothy J. Nelson,^{1b}
L. A. Ochrymowycz,^{1b} and D. B. Rorabacher^{*1a}

Contribution from the Departments of Chemistry, Wayne State University, Detroit, Michigan 48202, and the University of Wisconsin at Eau Claire, Eau Claire, Wisconsin 54701

Received December 14, 2006; E-mail: dbr@chem.wayne.edu

Abstract: The quinquedentate macrocyclic ligand cyclo-6,6′-[1,9-(2,5,8-trithianonane)]-2,2′-bipyridine ([15]aneS₃bpy = L), containing two pyridyl nitrogens and three thiaether sulfurs as donor atoms, has been synthesized and complexed with copper. The Cu^{II/I}L redox potential, the stabilities of the oxidized and reduced complex, and the oxidation and reduction electron-transfer kinetics of the complex reacting with a series of six counter reagents have been studied in acetonitrile at 25 °C, $\mu = 0.10$ M (NaClO₄). The Marcus cross relationship has been applied to the rate constants obtained for the reactions with each of the six counter reagents to permit the evaluation of the electron self-exchange rate constant, k_{11} . The latter value has also been determined independently from NMR line-broadening experiments. The cumulative data are consistent with a value of $k_{11} = 1 \times 10^5$ M⁻¹ s⁻¹, ranking this among the fastest-reacting Cu^{II/I} systems, on a par with the blue copper proteins known as cupredoxins. The resolved crystal structures show that the geometry of the Cu^{II}L and Cu^IL complexes are nearly identical, both exhibiting a five-coordinate square pyramidal geometry with the central sulfur donor atom occupying the apical site. The most notable geometric difference is a puckering of an ethylene bridge between two sulfur donor atoms in the Cu^IL complex. Theoretical calculations suggest that the reorganizational energy is relatively small, with the transition-state geometry more closely approximating the geometry of the Cu^{II}L ground state. The combination of a nearly constant geometry and a large self-exchange rate constant implies that this Cu^{II/I} redox system represents a true geometric “entatic state.”

Introduction

Much attention has been given to the unusual properties exhibited by the type-1 copper sites in blue copper proteins including their intense visible absorption peaks, unusual EPR hyperfine splitting, and high redox potentials.² However, from a functional standpoint, their most notable property is their rapid electron-transfer kinetics.^{3,4} NMR line-broadening measurements and related techniques have shown that the electron self-exchange rate constants (k_{11}) for several blue copper proteins (where L represents the coordinated protein)



containing a single type-1 copper site (cupredoxins) lie within the range of 10^5 – 10^6 M⁻¹ s⁻¹.^{5,6} By contrast, the majority of

inorganic Cu^{II/I} complexes exhibit significantly smaller k_{11} values in the range of 10^0 – 10^4 M⁻¹ s⁻¹,⁶ and Jordan and co-workers have found that the solvated Cu^{II/I} couple in water and in acetonitrile has values of $k_{11} < 10^{-6}$ M⁻¹ s⁻¹.⁷

Vallee and Williams were the first to emphasize that the electron-transfer lability of the blue copper proteins and other

- (1) (a) Wayne State University. (b) University of Wisconsin - Eau Claire.
(2) Dennison, C. *Coord. Chem. Rev.* **2005**, *249*, 3025–3054.
(3) Vallee, B. L.; Williams, R. J. P. *Proc. Natl. Acad. Sci. U.S.A.* **1968**, *59*, 498–505.
(4) (a) Holwerda, R. A.; Wherland, S.; Gray, H. B. *Ann. Rev. Biophys. Bioeng.* **1976**, *5*, 363–396. (b) Sykes, A. G. *Chem. Soc. Rev.* **1985**, *14*, 283–315. (c) Sykes, A. G. *Struct. Bonding* **1991**, *75*, 175–224. (d) Katz, A. K.; Shimoni-Livny, L.; Navon, O.; Navon, N.; Bock, C. W.; Glusker, J. P. *Helv. Chim. Acta* **2003**, *86*, 1320–1338.

- (5) (a) Dahlin, S.; Reinhammar, B.; Wilson, M. T. *Biochem. J.* **1984**, *218*, 609–614. (b) Groeneveld, C. M.; Canters, G. W. *Eur. J. Biochem.* **1985**, *153*, 559–564. (c) Groeneveld, C. M.; Dahlin, S.; Reinhammar, B.; Canters, G. W. *J. Am. Chem. Soc.* **1987**, *109*, 3247–3250. (d) Groeneveld, C. M.; Ouwerling, M. C.; Erkelens, C.; Canters, G. W. *J. Mol. Biol.* **1988**, *200*, 189–199. (e) Groeneveld, C. M.; Canters, G. W. *J. Biol. Chem.* **1988**, *263*, 167–173. (f) Lommen, A.; Canters, G. W. *J. Biol. Chem.* **1990**, *265*, 2768–2774. (g) Dennison, C.; Kyritsis, P.; McFarlane, W.; Sykes, A. G. *J. Chem. Soc., Dalton Trans.* **1993**, 1959–1963. (h) Dennison, C.; Kohzuma, T.; McFarlane, W.; Suzuki, S.; Sykes, A. G. *J. Chem. Soc., Dalton Trans.* **1994**, 437–443. (i) Kyritsis, P.; Dennison, C.; Ingledew, W. J.; McFarlane, W.; Sykes, A. G. *Inorg. Chem.* **1995**, *34*, 5370–5374. (j) Dennison, C.; Van, Driessche, G.; Van Beeumen, J.; McFarlane, W.; Sykes, A. G. *Chem. – Eur. J.* **1996**, *2*, 104–109. (k) Kyritsis, P.; Khozhuma [sic], T.; Sykes, A. G. *Biochim. Biophys. Acta* **1996**, *1295*, 245–252. (l) Dennison, C.; Kohzuma, T. *Inorg. Chem.* **1999**, *38*, 1491–1497. (m) Hunter, D. M.; McFarlane, W.; Sykes, A. G.; Dennison, C. *Inorg. Chem.* **2001**, *40*, 354–360. (n) van Amsterdam, I. M. C.; Ubbink, M.; Einsle, O.; Messerschmidt, A.; Merli, A.; Cavazzini, D.; Rossi, G. L.; Canters, G. W. *Nat. Struct. Biol.* **2002**, *9*, 48–52. (o) Dennison, C.; Lawler, A. T.; Kohzuma, T. *Biochemistry* **2002**, *41*, 552–560. (p) Sato, K.; Dennison, C. *Biochemistry* **2002**, *41*, 120–130. (q) Sato, K.; Kohzuma, T.; Dennison, C. *J. Am. Chem. Soc.* **2003**, *125*, 2101–2112. (r) Harrison, M. D.; Dennison, C. *ChemBioChem* **2004**, *5*, 1579–1581.
(6) Rorabacher, D. B. *Chem. Rev.* **2004**, *104*, 651–697.

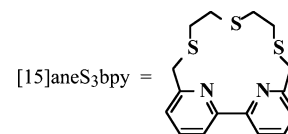
metalloenzymes might be the result of a structural *entatic* (i.e., strained) state in which the protein matrix constrains the metal coordination sphere to adopt a geometry closely approximating the transition state normally encountered in similar unconstrained systems, thereby minimizing the reorganization energy.^{3,8} Subsequent structural determinations for several cupredoxins^{9–13} have revealed that, in both the oxidized and reduced forms, the copper exists in a trigonal pyramidal coordination environment in which two unsaturated nitrogens (from histidines) and a mercaptide sulfur (cysteine) form the basal plane with an elongated bond to a thiaether sulfur (methionine) at the apical position.^{14,15} In some cupredoxins, such as azurins, a carbonyl oxygen (from glycine) is coordinated at the opposite apex to generate a distorted trigonal bipyramidal coordination sphere which is also maintained in both oxidation states.¹¹ A related red copper protein has a five-coordinate copper site exhibiting a square pyramidal coordination geometry.¹⁶

Both Solomon¹⁷ and Ryde¹⁸ and their co-workers have carried out theoretical calculations from which they concluded the spectral properties and electron-transfer kinetics of the cupre-

doxins are primarily attributable to the covalent nature of the Cu–S(mercaptide) bond in the basal plane of the active site. They also found that the electronic effects arising from this strong Cu–S bond give rise to the unusual geometry associated with the type-1 Cu site and also facilitate rapid electron transfer. The Cu atom can thus be viewed as existing in an *electronic entatic state* rather than a simple geometric constraint physically imposed upon the active site by the protein matrix.

The question remains as to whether geometric constraints alone can lead to rapid electron transfer in Cu^{II} systems. Several attempts have been reported in the literature, by Stanbury^{19–23} and others,^{24,25} to generate Cu^{II} complexes maintaining nearly constant geometries in both oxidation states. To date, none of these systems have yielded Cu^{II} self-exchange rate constants comparable to those exhibited by the rapidly reacting cupredoxins, and some have, in fact, yielded extremely small k_{11} values.^{19,20} By contrast, of the inorganic copper complexes that have been reported to exhibit the largest k_{11} values,^{26–30} all but one³⁰ involve the rupture of a single Cu–S(thiaether) bond upon reduction, a geometric change that is apparently quite facile.

In the current investigation, we have generated a quinque-dentate ligand incorporating three thiaether sulfurs and a bipyridine moiety within a macrocyclic structure, namely, cyclo-6,6′-[1,9-(2,5,8-trithianonane)]-2,2′-bipyridine ([15]aneS₃bpy = L).³¹ The coordination geometry of the oxidized complex, [Cu^{II}-



([15]aneS₃bpy)²⁺, is square pyramidal, paralleling the geometry of two rapidly reacting macrocyclic complexes, [Cu^{II}([15]-

- (7) (a) Sisley, M. J.; Jordan, R. B. *Inorg. Chem.* **1992**, *31*, 2880–2884. (b) Irangu, J.; Ferguson, M. J.; Jordan, R. B. *Inorg. Chem.* **2005**, *44*, 1619–1625.
- (8) Williams, R. J. P. *Inorg. Chim. Acta Rev.* **1971**, *5*, 137–155. Compare: Williams, R. J. P. *Eur. J. Biochem.* **1995**, *234*, 363–381.
- (9) Colman, P. M.; Freeman, H. C.; Guss, J. M.; Murata, M.; Norris, V. A.; Ramshaw, J. A. M.; Venkatappa, M. P. *Nature* **1978**, *272*, 319–324.
- (10) Plastocyanins: (a) Guss, J. M.; Freeman, H. C. *J. Mol. Biol.* **1983**, *169*, 521–563. (b) Guss, J. M.; Harrowell, P. R.; Murata, M.; Norris, V. A.; Freeman, H. C. *J. Mol. Biol.* **1986**, *192*, 361–387. (c) Collyer, C. A.; Guss, J. M.; Sugimura, Y.; Yoshizaki, F.; Freeman, H. C. *J. Mol. Biol.* **1990**, *211*, 617–632. (d) Guss, J. M.; Bartunik, H. D.; Freeman, H. C. *Acta Crystallogr., Sect. B* **1992**, *48*, 790–811. (e) Fields, B. A.; Bartsch, H. H.; Bartunik, H. D.; Cordes, F.; Guss, J. M.; Freeman, H. C. *Acta Crystallogr., Sect. D* **1994**, *50*, 709–730. (f) Bond, C. S.; Bendall, D. S.; Freeman, H. C.; Guss, J. M.; Howe, C. J.; Wagner, M. J.; Wilce, M. C. J. *Acta Crystallogr., Sect. D* **1999**, *55*, 414–421.
- (11) Azurins: (a) Baker, E. N. *J. Mol. Biol.* **1988**, *203*, 1071–1095. (b) Shepard, W. E. B.; Anderson, B. F.; Lewandowski, D. A.; Norris, G. E.; Baker, E. N. *J. Am. Chem. Soc.* **1990**, *112*, 7817–7819. (c) Nar, H.; Messerschmidt, A.; Huber, R.; van de Kamp, M.; Canters, G. W. *J. Mol. Biol.* **1991**, *221*, 765–772. (d) Li, C. M.; Inoue, T.; Gotowda, M.; Suzuki, S.; Yamaguchi, K.; Kai, K.; Kai, Y. *Acta Crystallogr., Sect. D* **1998**, *54*, 347–354. (e) Dodd, F. E.; Abraham, Z. H. L.; Eady, R. R.; Hasnain, S. S. *Acta Crystallogr., Sect. D* **2000**, *56*, 690–696.
- (12) Stellacyanin: Hart, P. J.; Nersissian, A. M.; Herrmann, R. G.; Nalbandyan, R. M.; Valentine, J. S.; Eisenberg, D. *Protein Sci.* **1996**, *5*, 2175–2183.
- (13) Other cupredoxins: (a) Pseudoazurin: Petrats, K.; Dauter, Z.; Wilson, K. S. *Acta Crystallogr., Sect. B* **1988**, *44*, 628–636. (b) Phytoeyanin (cucumber blue protein): Guss, J. M.; Merritt, E. A.; Phizackerley, R. P.; Freeman, H. C. *J. Mol. Biol.* **1996**, *262*, 686–705. Cf., Guss, J. M.; Merritt, E. A.; Phizackerley, R. P.; Hedman, B.; Murata, M.; Hodgson, K. O.; Freeman, H. C. *Science* **1988**, *241*, 806–811. (c) Rusticyanin: Harvey, I.; Hao, Q.; Duke, E. M. H.; Inglede, W. J.; Hasnain, S. S. *Acta Crystallogr., Sect. D* **1998**, *54*, 629–635. (d) Plantacyanin: Einsle, O.; Mehrabian, Z.; Nalbandyan, R.; Messerschmidt, A. *J. Biol. Inorg. Chem.* **2000**, *5*, 666–672. (e) Amicyanin: Mukherjee, M.; Maiti, S.; Ghosh, S.; Woolfson, M. M. *Acta Crystallogr., Sect. D* **2001**, *57*, 1276–1280. (f) Auracyanin: Bond, C. S.; Blankenship, R. E.; Freeman, H. C.; Guss, J. M.; Maher, M. J.; Selvaraj, F. M.; Wilce, M. C. J.; Willingham, K. M. *J. Mol. Biol.* **2001**, *306*, 47–67. Cf., Lee, M.; Maher, M. J.; Freeman, H. C.; Guss, J. M. *Acta Crystallogr., Sect. D* **2003**, *59*, 1545–1550.
- (14) Adman, E. T. *Adv. Protein Chem.* **1991**, *42*, 145–197.
- (15) In stellacyanin, a glutamine oxygen occupies the apical site; see ref 12.
- (16) Lieberman, R. L.; Arciero, D. M.; Hooper, A. B.; Rosenzweig, A. C. *Biochemistry* **2001**, *40*, 5674–5681.
- (17) (a) Solomon, E. I.; Lowery, M. D. *Science* **1993**, *259*, 1575–1581. (b) Guckert, J. A.; Lowery, M. D.; Solomon, E. I. *J. Am. Chem. Soc.* **1995**, *117*, 2817–2844. (c) Solomon, E. I.; Penfield, K. W.; Gewirth, A. A.; Lowery, M. D.; Shadle, S. E.; Guckert, J. A.; LaCroix, L. B. *Inorg. Chim. Acta* **1996**, *243*, 67–78. (d) Solomon, E. I.; LaCroix, L. B.; Randall, D. W. *Pure Appl. Chem.* **1998**, *70*, 799–808. (e) Solomon, E. I.; Lowery, M. D.; Guckert, J. A.; LaCroix, L. B. In *Electron Transfer Reactions; Advances in Chemistry Series*, Vol. 253; American Chemical Society: Washington, DC, 1997; pp 317–330. (f) Randall, D. W.; Gamelin, D. R.; LaCroix, L. B.; Solomon, E. I. *J. Biol. Inorg. Chem.* **2000**, *5*, 16–29. (g) Randall, D. W.; George, S. D.; Hedman, B.; Hodgson, K. O.; Fujisawa, K.; Solomon, E. I. *J. Am. Chem. Soc.* **2000**, *122*, 11620–11631. (h) Solomon, E. I.; Szilagy, R. K.; George, S. D.; Basumallick, L. *Chem. Rev.* **2004**, *104*, 419–458.
- (18) (a) Olsson, M. H. M.; Ryde, U.; Roos, B. O. *Protein Sci.* **1998**, *7*, 2659–2668. (b) De Kerpel, J. O. A.; Ryde, U. *Proteins: Struct., Func., Genet.* **1999**, *36*, 157–174. (c) Ryde, U.; Olsson, M. H. M.; Roos, B. O.; De Kerpel, J. O. A.; Pierloot, K. *J. Biol. Inorg. Chem.* **2000**, *5*, 565–574. (d) Ryde, U.; Olsson, M. H. M. *Int. J. Quantum Chem.* **2001**, *81*, 335–347. (e) Ryde, U.; Olsson, M. H. M.; Roos, B. O.; Borin, A. C. *Theor. Chem. Acc.* **2001**, *105*, 452–462. (f) Sigfridsson, E.; Olsson, M. H. M.; Ryde, U. *J. Phys. Chem. B* **2001**, *105*, 5546–5552.
- (19) Xie, B.; Elder, T.; Wilson, L. J.; Stanbury, D. M. *Inorg. Chem.* **1999**, *38*, 12–19.
- (20) Xie, B.; Wilson, L. J.; Stanbury, D. M. *Inorg. Chem.* **2001**, *40*, 3606–3614.
- (21) Goodwin, J. A.; Stanbury, D. M.; Wilson, L. J.; Eigenbrot, C. W.; Scheidt, W. R. *J. Am. Chem. Soc.* **1987**, *109*, 2979–2991.
- (22) Goodwin, J. A.; Wilson, L. J.; Stanbury, D. M.; Scott, R. A. *Inorg. Chem.* **1989**, *28*, 42–50.
- (23) Coggin, D. K.; González, J. A.; Kook, A. M.; Bergman, C.; Brennan, T. D.; Scheidt, W. R.; Stanbury, D. M.; Wilson, L. J. *Inorg. Chem.* **1991**, *30*, 1125–1134.
- (24) Metelski, P. D.; Hinman, A. S.; Takagi, H. D.; Swaddle, T. W. *Can. J. Chem.* **1995**, *73*, 61–69.
- (25) McMaster, J.; Beddoes, R. L.; Collison, D.; Eardley, D. R.; Helliwell, M.; Garner, C. D. *Chem. Eur. J.* **1996**, *2*, 685–693.
- (26) Vande Linde, A. M. Q.; Juntunen, K. L.; Mols, O.; Ksebaty, M. B.; Ochrymowycz, L. A.; Rorabacher, D. B. *Inorg. Chem.* **1991**, *30*, 5037–5042.
- (27) Vande Linde, A. M. Q.; Westerby, B. C.; Ochrymowycz, L. A.; Rorabacher, D. B. *Inorg. Chem.* **1993**, *32*, 251–257.
- (28) Krylova, K.; Kulatilleke, C. P.; Heeg, M. J.; Salhi, C. A.; Ochrymowycz, L. A.; Rorabacher, D. B. *Inorg. Chem.* **1999**, *38*, 4322–4328.
- (29) Leggett, G. H.; Dunn, B. C.; Vande Linde, A. M. Q.; Ochrymowycz, L. A.; Rorabacher, D. B. *Inorg. Chem.* **1993**, *32*, 5911–5918.
- (30) Pulliam, E. J.; McMillin, D. R. *Inorg. Chem.* **1984**, *23*, 1172–1175. TAAB = tetrabenzob[*b,f,j,n*]-[1,5,9,13]tetraazacyclohexadecene.
- (31) This ligand can also be designated as 2,5,8[9](6,6′)2,2′-bipyridinophane based on the nomenclature adopted by Weber and Vögtle for similar macrocyclic ligands containing pyridines and thiaether sulfurs: Weber, E.; Vögtle, F. *Liebigs Ann. Chem.* **1976**, 891–915.

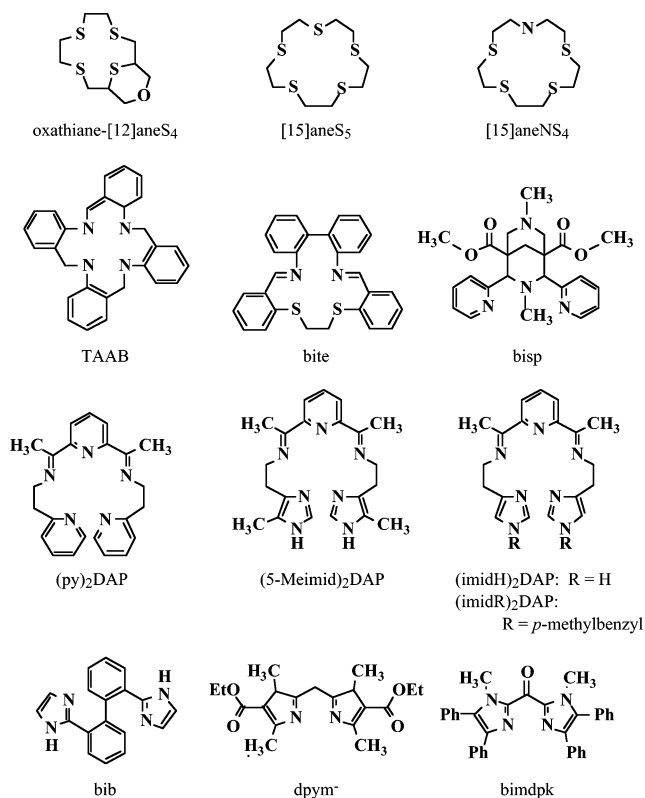


Figure 1. Ligands mentioned in this work.

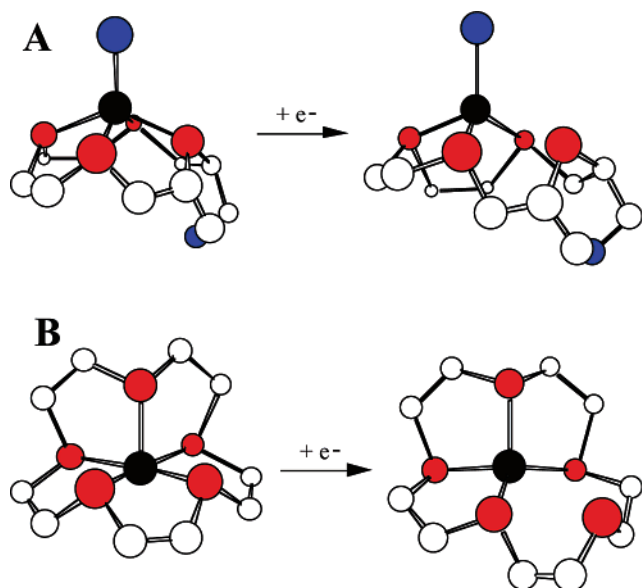


Figure 2. Schematic representation of geometric changes observed to accompany electron transfer for (A) [Cu^{II}](14]aneS₄)] (top) and (B) [Cu^{II}](15]aneS₅)] (bottom). Atom designations are as follows: black = Cu, red = S, blue = O, white = C. Hydrogen atoms have been omitted for clarity.

aneS₅)]²⁺ and [Cu^{II}](15]aneNS₄)]²⁺ (see Figure 1) which are among the handful of inorganic systems exhibiting values of $k_{11} \geq 10^5 \text{ M}^{-1} \text{ s}^{-1}$. Both of these latter complexes involve the rupture of a labile Cu–S(thiaether) bond in the front of the basal plane (Figure 2) to generate a tetrahedral Cu^IL species.^{26,27} In the current system, the more rigid bipyridine moiety makes it difficult to rupture a Cu–N bond in the frontal portion of the

basal plane, and a crystal structure of the reduced [Cu^I](15]aneS₃bpy)]⁺ complex shows the geometry to be five-coordinate, little changed from that of the oxidized species. The nearly invariant geometry for the two oxidation states meets the criterion defined by Vallee and Williams in their original concept of a geometric entatic state.³ Reduction and oxidation cross-reaction kinetic studies as well as NMR line-broadening measurements have been conducted on this system in acetonitrile, yielding the largest self-exchange rate constant reported to date for a coordination-invariant Cu^{II/I} system devoid of a Cu–mercaptide sulfur bond.

In support of the current investigation, theoretical calculations employing density functional theory (DFT) were carried out to determine the relative energy barrier associated with the small ligand reorganization accompanying electron transfer in [Cu^{II/I}](15]aneS₃bpy)]^{2+/+}. The results of these calculations provide insight into the probable reaction pathway for the overall electron-transfer reaction. Additional calculations have also been made on previously reported coordination-invariant Cu^{II/I} systems for comparative purposes.

Experimental Section

Ligand Synthesis. The synthesis of [15]aneS₃bpy was carried out using the generalized high-dilution cyclocondensation methodology employed to prepare macrocyclic polythiaethers, including the general separation and characterization techniques previously described.³³ The essential synthon—6,6′-bis(chloromethyl)-2,2′-bipyridine—was prepared by chlorination of 6,6′-dimethyl-2,2′-bipyridine,³⁴ which in turn was prepared by the in situ generated nickel(0) coupling of 2-bromo-6-methylpyridine.³⁵ In 0.5 L of anhydrous DMF were dissolved 16.0 g (0.063 mol) of 6,6′-bis(chloromethyl)-2,2′-bipyridine along with 9.8 g (0.063 mol) of 2-mercaptoethyl sulfide (Aldrich Chemical Co., #M400–7). The solution was added under an argon atmosphere at a rate of 0.5 mL/min to a stirred suspension of 20.7 g (0.15 mol) of powdered anhydrous potassium carbonate in 1 L of DMF, maintained at 85–100 °C for the reaction duration. The filter cake and vacuum evaporation residue from the reaction were dispersed in 1 L of methylene chloride and washed with three 300-mL portions of 2 M sodium chloride brine, dried with MgSO₄, and vacuum filtered and reconcentrated to 21 g of semisolid amber residue. The residue was flash eluted to remove higher polymers with 1.3 L of toluene through a 3 × 40 cm silica gel column. The 13 g of recovered elution residue were fractionally chromatographed with 50:50 toluene/hexane through a 3 cm × 50 cm silica gel column. By TLC analysis the major product fractions, $R_f = 0.55$, 5:95 ethyl acetate/toluene, were combined and recrystallized twice from 30:70 toluene/hexane to yield 5.13 g (24.4%) of colorless plates, mp = 149–151 °C. ¹³C NMR (100.6 MHz, CDCl₃) δ in ppm (multiplicity): 31.99 (t), 32.79 (t), 36.63 (t), 120.01 (d), 122.54 (d), 137.74 (d), 155.10 (s), 160.51 (s). EI-MS, m/z (relative intensity): 334 M⁺ (67), 301 (14), 273 (88), 248 (100), 214 (78), 184 (33), 154 (19); electrospray MS, m/z : 335.100 MH⁺, 357.06 MNa⁺, 373.04 MK⁺, 691.00 M₂Na⁺. Anal. Calcd for C₁₆H₁₈N₂S₃: C = 57.45; H = 5.42, S = 28.76. Found: C = 57.22, H = 5.40; S = 28.50.

Reagents. The reducing agent [Co^{II}(dmg)₃(BC₆H₅)₂] (dmg = dimethylglyoxime; BC₆H₅²⁺ = phenylborate ion) was prepared using the method of Borchardt and Wherland³⁶ as modified by Stanbury and co-workers.¹⁹ All other counter reagents were prepared by literature

(32) Corfield, P. W. R.; Ceccarelli, C.; Glick, M. D.; Moy, I. W.-Y.; Ochrymowycz, L. A.; Rorabacher, D. B. *J. Am. Chem. Soc.* **1985**, *107*, 2399–2404.

(33) Aronne, L.; Dunn, B. C.; Vyvyan, J. R.; Souvignier, C. W.; Mayer, M. J.; Howard, T. A.; Salhi, C. A.; Goldie, S. N.; Ochrymowycz, L. A.; Rorabacher, D. B. *Inorg. Chem.* **1995**, *34*, 357–369.

(34) Newkome, G. R.; Puckett, W. E.; Kiefer, G. E.; Gupta, V. K.; Xia, Y.; Coreil, M.; Hackney, M. A. *J. Org. Chem.* **1982**, *47*, 4116–4120.

(35) Tiecco, M.; Testaferri, L.; Tingoli, M.; Chianelli, D.; Montanucci, M. *Synthesis* **1984**, 736–738.

(36) Borchardt, D.; Wherland, S. *Inorg. Chem.* **1986**, *25*, 901–905.

methods as previously described.^{37–39} Copper(II) perchlorate was prepared by the slow addition of perchloric acid to solid copper carbonate⁴⁰ on an ice bath and was then recrystallized from acetonitrile to remove the waters of hydration. (**Warning!** All metal perchlorate salts are potentially explosive and should be handled with extreme care. These compounds should be prepared in small quantities and should never be dried.) Copper(I) perchlorate was prepared by crystallization from acetonitrile using the method of Hathaway et al.⁴¹ All aqueous solutions were prepared using conductivity grade distilled–deionized water. Acetonitrile solutions were prepared with HPLC grade solvent (Fisher Scientific) which has been shown to contain less than 0.02% water (by wt).³⁸ The addition of small amounts of added water had no effect upon the experimental results; therefore, no attempt was made to reduce the residual water content. The concentrations of all counter reagent solutions were determined spectrophotometrically. Copper solutions in both water and acetonitrile were first oxidized to Cu^{II} and then standardized by EDTA titration. Ligand solutions were standardized by potentiometric titrations with a standard mercury(II) solution using a mercury pool indicating electrode.

X-Ray Structural Determinations. Diffraction data for [Cu^{II}-(15)aneS₃bpy](ClO₄)₂ were collected on a Bruker P4/CCD diffractometer equipped with Mo radiation and a graphite monochromator at room temperature. Data collection proceeded on a red needle approximately 0.4 × 0.06 × 0.04 mm³. A sphere of data was measured at 10 s/frame and 0.3° between frames. A total of 1650 frames was collected, yielding 14834 reflections, of which 4876 were independent. The frame data were indexed and integrated with the manufacturer's SMART, SAINT, and SADABS software.⁴² All structures were refined using Sheldrick's SHELX-97 software.⁴³ The hydrogen atoms were placed in calculated positions. All samples examined exhibited some degree of twinning, and this best data set was the result of the extraction of the major component with the program GEMINI. The complex crystallizes with two perchlorate counterions.

Diffraction data for the [Cu^I[(15)aneS₃bpy]]ClO₄ complex were measured on a Bruker APEX-II κ geometry diffractometer⁴² with Mo radiation and a graphite monochromator at 100 K. A green-brown rod approximately 0.45 × 0.08 × 0.08 mm³ was used for data collection. A total of 1083 frames was collected at 10 s/frame, yielding 12392 reflections of which 4463 were independent. Frames were collected as a series of sweeps with the detector at 40 mm and 0.3° between each frame. Hydrogen atoms were placed in observed positions. The complex crystallizes with one perchlorate counterion, which showed typical perchlorate disorder. The oxygen atoms were modeled in partially occupied sites held isotropic.

NMR Measurements. The NMR spectrum for [Cu^I[(15)aneS₃bpy]]⁺ and line-broadening measurements in deuterated acetonitrile were made with a Mercury 400 NMR spectrometer using an appropriate pulse sequence. A solution of Cu^IL was prepared by comproportionation by stirring a Cu^{II}L solution with excess fine copper shot. The solution was then decanted, and the resultant Cu^IL concentration was determined spectrophotometrically at 390 nm.

- (37) (a) [Ru(NH₃)₅isn](ClO₄)₂: Kuehn, C. G.; Taube, H. *J. Am. Chem. Soc.* **1976**, *98*, 689–702. (b) [Ru(NH₃)₅py](ClO₄)₂: Gaunder, R. G.; Taube, H. *Inorg. Chem.* **1970**, *9*, 2627–2639, with modifications as described by Cummins, D.; Gray, H. B. *J. Am. Chem. Soc.* **1977**, *99*, 5158–5167. (c) [Ru(NH₃)₅bpy](ClO₄)₂: Brown, G. M.; Sutin, N. *J. Am. Chem. Soc.* **1979**, *101*, 883–892. (d) [Co(bpy)₃](ClO₄)₂: Burstall, F. H.; Nyholm, R. S. *J. Chem. Soc.* **1952**, 3570–3579; [Co(phen)₃](ClO₄)₂ was prepared by an analogous approach.
- (38) Dunn, B. C.; Ochrymowycz, L. A.; Rorabacher, D. B. *Inorg. Chem.* **1995**, *34*, 1954–1956.
- (39) Meagher, N. E.; Juntunen, K. L.; Salhi, C. A.; Ochrymowycz, L. A.; Rorabacher, D. B. *J. Am. Chem. Soc.* **1992**, *114*, 10411–10420.
- (40) Cooper, T. H.; Mayer, M. J.; Leung, K.-H.; Ochrymowycz, L. A.; Rorabacher, D. B. *Inorg. Chem.* **1992**, *31*, 3796–3804.
- (41) Hathaway, B. J.; Holah, D. G.; Postlethwaite, J. D. *J. Chem. Soc.* **1961**, 3215–3218.
- (42) APEX II, SMART, SAINT, GEMINI and SADABS collection and processing programs are distributed by the manufacturer: Bruker AXS Inc., Madison, WI.
- (43) Sheldrick, G. SHELX-97; University of Göttingen: Germany, 1997.

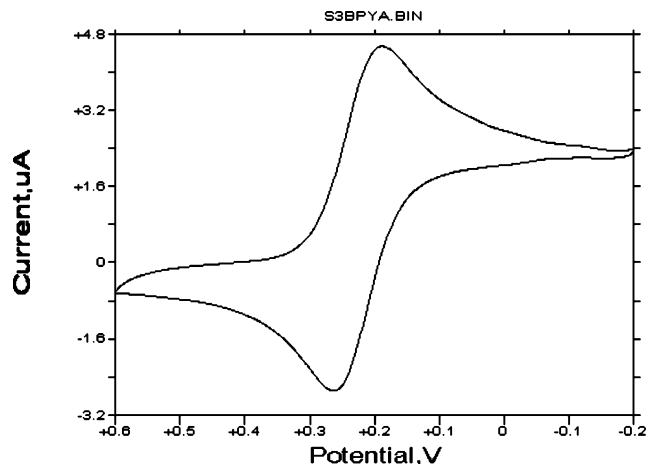


Figure 3. Cyclic voltammogram for [Cu^{II}[(15)aneS₃bpy]] in acetonitrile at ambient temperature, $\mu = 0.10$ M (ClO₄⁻), $\nu = 20$ mV s⁻¹. Potentials shown are vs Ag/AgCl reference electrode ($E_{1/2} = -0.127$ V vs ferrocene).

Instrumentation. The potentials of all reagents were determined by slow-scan cyclic voltammetry (CV) in acetonitrile using a BAS-100 electrochemical analyzer (Bioanalytical Systems, West Lafayette, IN) equipped with a 3-mm glassy-carbon-disk working electrode, a platinum wire auxiliary electrode, and an aqueous Ag/AgCl reference electrode. Ferrocene (Sigma Chemical Co) was used as an internal or external standard. All kinetic measurements were made using a Durrum D-110 stopped-flow spectrophotometer that incorporated a modified flow system from Tritech Scientific Ltd. (Winnipeg, Manitoba, Canada) with an A/D interface to a PC. The modified flow system contained all Kel-F and glass fittings to prevent degradation when using acetonitrile as the solvent. This instrument was thermostatted at 25.0 ± 0.2 °C, using a circulating constant temperature bath. Ionic strength was maintained at 0.10 M using NaClO₄ recrystallized from acetonitrile.

Computational Details. All calculations were performed using the development version of the Gaussian suite⁴⁴ employing the TPSS meta-GGA density functional.⁴⁵ Scalar-relativistic effects were taken into account via the relativistic effective-core potential of Dolg et al. for the copper center,⁴⁶ while spin–orbit effects have been ignored. Ligand orbitals were described by the 6-311+G(d) basis set.^{47–51} Geometries were optimized for all Cu^I and Cu^{II} complexes using the Bery algorithm.⁵² Analytic harmonic vibrational frequencies were computed to ensure that the optimized structures were minima on the potential energy surface and to provide zero-point energy corrections.

Results

Redox Potentials. As illustrated in Figure 3, the cyclic voltammogram for [Cu^{II}[(15)aneS₃bpy]]^{2+/+} is reversible at slow scan rates (20 mV s⁻¹) in acetonitrile with a value of $E_{1/2} = -0.127$ V vs ferrocene (Fc).^{53,54} Formal potential values for [Ru^{III/II}(NH₃)₅py]^{3+/2+}, [Co^{III/II}(phen)₃]^{3+/2+}, and [Co^{III/II}(bpy)₃]^{3+/2+}

- (44) Frisch, M. J.; et al. *Gaussian DV*, revision E.05; Gaussian, Inc.: Wallingford, CT, 2006. [See Supporting Information for complete list of authors.]
- (45) Tao, J. M.; Perdew, J. P.; Staroverov, V. N.; Scuseria, G. E. *Phys. Rev. Lett.* **2003**, *91*, 146401.
- (46) Dolg, M.; Wedig, U.; Stoll, H.; Preuss, H. *J. Chem. Phys.* **1987**, *86*, 866–872.
- (47) Curtiss, L. A.; McGrath, M. P.; Blauadeau, J. P.; Davis, N. E.; Binning, R. C., Jr.; Radom, L. *J. Chem. Phys.* **1995**, *103*, 6104–6113.
- (48) Krishnan, R.; Binkley, J. S.; Seeger, R.; Pople, J. A. *J. Chem. Phys.* **1980**, *72*, 650–654.
- (49) McGrath, M. P.; Radom, L. *J. Chem. Phys.* **1991**, *94*, 511–516.
- (50) McLean, A. D.; Chandler, G. S. *J. Chem. Phys.* **1980**, *72*, 5639–5648.
- (51) Binning, R. C., Jr.; Curtiss, L. A. *J. Comp. Chem.* **1990**, *11*, 1206–1216.
- (52) Schlegel, H. B. *J. Comp. Chem.* **1982**, *3*, 214–218.
- (53) The use of ferrocene as a standard for potentials in nonaqueous media follows the recommendations of the International Union of Pure and Applied Chemistry (IUPAC): Gritzner, G.; Kuta, J. *Pure Appl. Chem.* **1984**, *56*, 461–466.

Table 1. Physical Parameters for All Reagents in Acetonitrile at 25 °C, $\mu = 0.10$ M

reagent ^a	E^f V vs Fc	$10^8 r^b$ cm	λ_{\max} nm	$10^{-3} \epsilon$ $M^{-1} \text{cm}^{-1}$	k_{22} $M^{-1} \text{s}^{-1}$
$[\text{Cu}^{\text{II}}([\text{15}] \text{aneS}_3 \text{bpy})]^{2+/+}$	-0.127 ^c	4.4 ^c	390 ^c	2.54 ^c	
Reductants					
$[\text{Ru}^{\text{II}}(\text{NH}_3)_5 \text{py}]^{2+}$	-0.088 ^c	3.8 ^d	407 ^e	7.8 ^e	4.7×10^5 ^d
$[\text{Co}^{\text{II}}(\text{dmg})_2(\text{BC}_6\text{H}_5)_2]$	-0.212 ^f	5.9 ^g	354 ^f	6.05 ^f	1.18×10^2 ^f
Oxidants					
$[\text{Ru}^{\text{III}}(\text{NH}_3)_4 \text{bpy}]^{3+/+}$	0.127 ^h	4.4 ⁱ	522 ^e	3.31 ^e	5.5×10^5 ^h
$[\text{Ru}^{\text{III}}(\text{NH}_3)_5 \text{isn}]^{3+/+}$	-0.012 ^h	3.8 ^e	478 ^j	11.9 ^j	4.7×10^5 ^h
$[\text{Co}^{\text{III}}(\text{phen})_3]^{3+/+}$	-0.035 ^c	7.0 ^k	330 ^l	4.68 ^l	1.28 ^c
$[\text{Co}^{\text{III}}(\text{bpy})_3]^{3+/+}$	-0.076 ^c	7.0 ^k	317 ^m	31.2 ^m	0.645 ^h

^a For ligand abbreviations, see text. ^b Effective ionic radius. ^c This work. ^d Assumed to be identical to the corresponding isonicotinamide complex. ^e Reference 37c. ^f Reference 36. ^g Murguia, M. A.; Wherland, S. *Inorg. Chem.* **1991**, *30*, 139–144. ^h Dunn, B. C.; Ochrymowycz, L. A.; Rorabacher, D. B. *Inorg. Chem.* **1997**, *36*, 3253–3257. ⁱ Reference 60. ^j Shepherd, R. E.; Taube, H. *Inorg. Chem.* **1973**, *12*, 1392–1401. ^k Tsukahara, K.; Wilkins, R. G. *Inorg. Chem.* **1985**, *24*, 3399–3402. ^l Przystas, T. J.; Sutin, N. *J. Am. Chem. Soc.* **1973**, *95*, 5545–5546. ^m Martin, B.; Waind, G. M. *J. Chem. Soc.* **1958**, 4284–4288.

in acetonitrile (py = pyridine; phen = 1,10-phenanthroline; bpy = 2,2'-bipyridine) were determined in a similar fashion as part of the current work. Potential values for $[\text{Ru}^{\text{III}}(\text{NH}_3)_4 \text{bpy}]^{3+/2+}$,³⁸ $[\text{Ru}^{\text{III}}(\text{NH}_3)_5 \text{isn}]^{3+/2+}$,³⁸ and $[\text{Co}^{\text{III}}(\text{dmg})_3(\text{BC}_6\text{H}_5)_2]^{+/0}$ ¹⁹ were taken from the literature (isn = isonicotinamide, dmg = dimethylglyoxime). The physical parameters for all reagents used in this work are listed in Table 1.

Stability Constants. As noted in reports on previously studied $\text{Cu}^{\text{II}}\text{L}$ systems,^{33,55} the stability of $\text{Cu}^{\text{II}}\text{L}$ complexes is enhanced in acetonitrile relative to water, whereas the affinity of Cu^{I} for acetonitrile causes the reduced complexes to decrease in stability. The diminished stability of the $[\text{Cu}^{\text{I}}([\text{15}] \text{aneS}_3 \text{bpy})]^+$ complex, combined with its sizable absorbance in the vicinity of 390 nm, made it possible to determine the stability constant of the reduced complex in acetonitrile by the spectrophotometric approach of McConnell and Davidson⁵⁶ as represented by the relationship:⁵⁷

$$\frac{bC_L}{A} = \frac{1}{\epsilon_{\text{Cu}^{\text{I}}\text{L}}} + \frac{1}{\epsilon_{\text{Cu}^{\text{II}}\text{L}} K_{\text{Cu}^{\text{II}}\text{L}}' [\text{Cu}^{\text{I}}]} \quad (2)$$

In this expression, b represents the cell path length, C_L is the total ligand concentration in solution, $\epsilon_{\text{Cu}^{\text{I}}\text{L}}$ is the molar absorptivity of the reduced complex, $K_{\text{Cu}^{\text{II}}\text{L}}'$ is the conditional $\text{Cu}^{\text{I}}\text{L}$ stability constant,⁵⁸ and $[\text{Cu}^{\text{I}}]$ is the concentration of uncomplexed copper(I). Because the value of $[\text{Cu}^{\text{I}}]$ was not known initially, the total Cu^{I} concentration ($C_{\text{Cu}^{\text{I}}}$) was substituted

- (54) For comparison, the potential values for $[\text{Cu}^{\text{II}}([\text{15}] \text{aneS}_3)]^{2+/+}$ and $[\text{Cu}^{\text{II}}([\text{15}] \text{aneNS}_4)]^{2+/+}$ are about 0.31 and 0.09 V vs ferrocene, respectively, based on (a) their potential values relative to $[\text{Cu}^{\text{II}}([\text{14}] \text{aneS}_4)]^{2+/+}$ in aqueous solution [0.68, 0.457, and 0.58 V (vs SHE), respectively; Bernardo, M. M.; Heeg, M. J.; Schroeder, R. R.; Ochrymowycz, L. A.; Rorabacher, D. B. *Inorg. Chem.* **1992**, *31*, 191–198] and (b) the potential of the latter system in acetonitrile [0.205 V (vs Fc); ref 38].
- (55) Kulatilleke, C. P.; Goldie, S. N.; Ochrymowycz, L. A.; Rorabacher, D. B. *Inorg. Chem.* **1999**, *38*, 5906–5909.
- (56) McConnell, H.; Davidson, N. *J. Am. Chem. Soc.* **1950**, *72*, 3164–3167. Compare: Benesi, H. A.; Hildebrand, J. H. *J. Am. Chem. Soc.* **1949**, *71*, 2703–2707.
- (57) Sokol, L. S. W. L.; Ochrymowycz, L. A.; Rorabacher, D. B. *Inorg. Chem.* **1981**, *20*, 3189–3195.
- (58) The conditional stability constant, $K_{\text{Cu}^{\text{II}}\text{L}}'$, includes any adducts of $\text{Cu}^{\text{II}}\text{L}$ formed with perchlorate ion as previously documented for $\text{Cu}^{\text{II}}\text{L}$ complexes in water; ref 40. Compare: Nazarenko, A. Y.; Izatt, R. M.; Lamb, J. D.; Desper, J. M.; Matysik, B. E.; Gellman, S. H. *Inorg. Chem.* **1992**, *31*, 3990–3993.

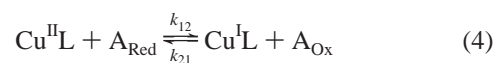
for this term to obtain an initial estimate of $K_{\text{Cu}^{\text{I}}\text{L}}'$; this estimated stability constant value was then used to correct for the amount of uncomplexed Cu^{I} (i.e., $[\text{Cu}^{\text{I}}] = C_{\text{Cu}^{\text{I}}} - [\text{Cu}^{\text{I}}\text{L}]$) in an iterative manner until a consistent value of $K_{\text{Cu}^{\text{I}}\text{L}}'$ was obtained. In the presence of large Cu^{I} concentrations, the absorbance values tended to decrease abnormally, thereby causing a plot of bC_L/A vs $[\text{Cu}^{\text{I}}]^{-1}$ to become nonlinear. After extensive investigation, it was determined that this problem resulted from an apparent autoxidation of the $\text{Cu}^{\text{I}}\text{L}$ complex under these conditions (perhaps by O_2) since the initial absorbance could be regenerated upon electrolysis. Therefore, data from solutions containing large $[\text{Cu}^{\text{I}}]$ values were not included in the final data analysis. From the linear portion of the plot of eq 2, the slope and intercept yielded the following values in acetonitrile at 25.0 °C, $\mu = 0.10$ (ClO_4^-): $K_{\text{Cu}^{\text{I}}\text{L}}' = (3.15 \pm 0.14) \times 10^4 \text{ M}^{-1}$, $\epsilon_{\text{Cu}^{\text{I}}\text{L}} = (2.72 \pm 0.04) \times 10^3 \text{ M}^{-1} \text{cm}^{-1}$ (390 nm). (This value is similar to that found for $[\text{Cu}^{\text{I}}([\text{14}] \text{aneS}_4)]^{2+}$ in acetonitrile: $K_{\text{Cu}^{\text{I}}\text{L}}' = 1.7 \times 10^4 \text{ M}^{-1}$.)³³ An independent measurement of the molar absorptivity was obtained by adding large excess amounts of ligand to solutions of Cu^{I} . A series of such measurements yielded an average value of $\epsilon_{\text{Cu}^{\text{I}}\text{L}} = 2.54 \times 10^3 \text{ M}^{-1} \text{cm}^{-1}$. The latter value was used for all subsequent calculations.

The stability constant for the oxidized complex in acetonitrile was calculated from the measured $\text{Cu}^{\text{II}}\text{L}$ redox potential using the Nernst equation in the form,

$$E^f = E_{\text{solvent}}^0 - \frac{2.303RT}{n\mathcal{F}} \log \frac{K_{\text{Cu}^{\text{II}}\text{L}}'}{K_{\text{Cu}^{\text{I}}\text{L}}'} \quad (3)$$

where E^f represents the formal potential value obtained in acetonitrile (vs ferrocene) for the $\text{Cu}^{\text{II}}\text{L}$ redox couple from slow-scan cyclic voltammetry, $E_{\text{solvent}}^0 = 0.660$ V (vs ferrocene) represents the potential for the solvated Cu^{II} couple in acetonitrile obtained in a similar manner in 0.10 M NaClO_4 , and the other terms have their conventional meanings. Equation 3 yielded a value of $K_{\text{Cu}^{\text{II}}\text{L}}' = 6.3 \times 10^{17} \text{ M}^{-1}$.

Reaction Kinetics. The kinetics for $\text{Cu}^{\text{I}}\text{L}$ oxidation were studied with a series of four oxidants (A_{Ox}); and the kinetics of the reduction reactions for $\text{Cu}^{\text{II}}\text{L}$ were similarly measured using two counter reductants (A_{Red}) according to the general reaction:



The reactions involving the oxidation of $\text{Cu}^{\text{I}}\text{L}$ by $[\text{Co}^{\text{III}}(\text{phen})_3]^{3+/+}$ and $[\text{Co}^{\text{III}}(\text{bpy})_3]^{3+/+}$ were run under pseudo-first-order conditions with the counter reagent present in excess. For reactions in which the cobalt reagent was present in less than 10-fold excess, only the initial portion of the reaction was used in analyzing the data. Pseudo-first-order conditions were also used in studying the $\text{Cu}^{\text{II}}\text{L}$ reduction kinetics with $[\text{Co}^{\text{II}}(\text{dmg})_3(\text{BC}_6\text{H}_5)_2]$ except that, in that case, the $\text{Cu}^{\text{II}}\text{L}$ species was present in large excess. The reduction study involving $\text{Cu}^{\text{II}}\text{L}$ reacting with $[\text{Ru}^{\text{II}}(\text{NH}_3)_5 \text{py}]^{2+}$ and the oxidation studies in which $[\text{Ru}^{\text{III}}(\text{NH}_3)_4 \text{bpy}]^{3+/+}$ and $[\text{Ru}^{\text{III}}(\text{NH}_3)_5 \text{isn}]^{3+/+}$ served as the counter reagents were carried out under second-order conditions, the latter two reactions being very rapid. Each reaction was run approximately 10 times for each set of reaction concentrations. The resolved second-order rate constants obtained for all six cross-reactions are listed in Table 2. (Individual rate constant data may be accessed as Supporting Information.)

Table 2. Cross-Reaction Rate Constants and Experimental and Calculated Self-Exchange Rate Constants in Acetonitrile at 25 °C, $\mu = 0.10$ M

reagent	$10^{-6} k_{12}$ OR k_{21} ($M^{-1} s^{-1}$) ^a	$\log k_{11}$ ($M^{-1} s^{-1}$)
NMR line-broadening		5.3, 5.6
	Reductions	
[Ru ^{II} (NH ₃) ₅ py] ²⁺	0.21(3)	5.07
[Co ^{II} (dmg) ₂ (BC ₆ H ₅) ₂]	0.0167(6)	4.54
	Oxidations	
[Ru ^{III} (NH ₃) ₄ bpy] ³⁺	29(16)	5.19
[Ru ^{III} (NH ₃) ₅ isn] ³⁺	3.2(4)	5.01
[Co ^{III} (phen) ₃] ³⁺	0.00159(6)	4.80
[Co ^{III} (bpy) ₃] ³⁺	0.00055(1)	4.76

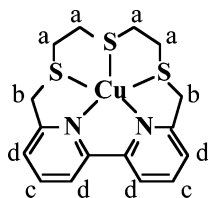
^a Values in parentheses represent standard deviations in terms of the last digits shown: e.g., 0.21(3) = 0.21 ± 0.03.

Self-Exchange Rate Constant Values. The second-order cross-reaction rate constants, k_{12} and k_{21} , were inserted into the Marcus cross-relationship⁵⁹ as rearranged to the form,⁶

$$k_{11} = \frac{(k_{12})^2}{k_{22}K_{12}f_{12}(W_{12})^2} \quad \text{OR} \quad k_{11} = \frac{(k_{21})^2}{k_{22}K_{21}f_{21}(W_{21})^2} \quad (5)$$

to obtain estimates of the electron self-exchange rate constant for the [Cu^{II}/([15]aneS₃bpy)]^{2+/+} redox couple, k_{11} , from each of the six cross-reactions. The individual terms in eq 5 include the self-exchange rate constant for each counter reagent, k_{22} (Table 2), and the reaction equilibrium constant, K_{12} or K_{21} , as calculated from the difference in the redox potentials of the two reactants involved (Table 2). Of the remaining terms, f_{12} and f_{21} represent nonlinear correction terms, and W_{12} and W_{21} are electrostatic work terms that can be calculated as previously described.^{39,60} The values for the effective ionic radius (r) for each reactant, as used to calculate the work term values,⁶⁰ are included in Table 1. (It should be noted that the k_{11} value obtained from the oxidation of Cu^IL by [Ru^{III}(NH₃)₄bpy]³⁺ is the least reliable since the reaction rate constant was exceptionally large ($k_{21} \approx 10^7 M^{-1} s^{-1}$) relative to the detection limits of the stopped-flow instrument used.)⁶¹

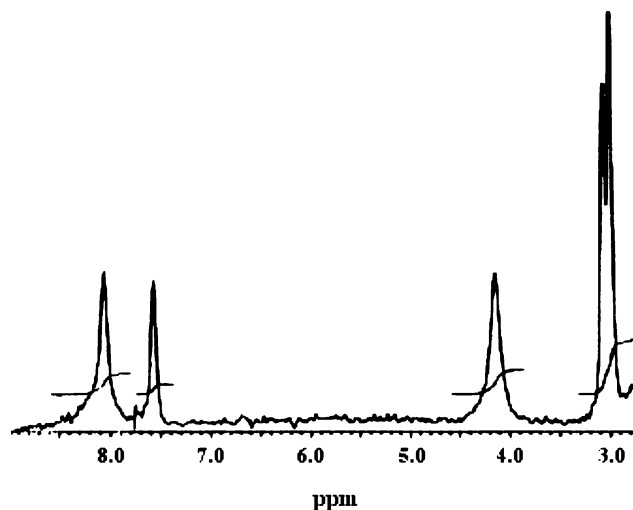
NMR Measurements. As illustrated in Figure 4, the NMR spectrum of [Cu^I([15]aneS₃bpy)]⁺ exhibits a doublet centered at 3.1 ppm (a) and singlets at 4.2 (b), 7.6 (c), and 8.1 ppm (d) with peak ratios of 4:2:1:2, respectively. This spectrum is consistent with the peak assignments shown below assuming full complexation by all five donor atoms: A limited independent



(59) Marcus, R. A.; Sutin, N. *Biochim. Biophys. Acta.* **1985**, *811*, 265–322.

(60) Martin, M. J.; Endicott, J. F.; Ochrymowycz, L. A.; Rorabacher, D. B. *Inorg. Chem.* **1987**, *26*, 3012–3022.

(61) We have previously demonstrated our ability to measure second-order rate constants as large as $10^8 M^{-1} s^{-1}$: Dunn, B. C.; Meagher, N. E.; Rorabacher, D. B. *J. Phys. Chem.* **1996**, *100*, 16925–16933. However, the current measurements in acetonitrile were carried out using an instrument that was modified for use with acetonitrile. This instrument has a significantly slower mixing time (~10 ms), thereby reducing our ability to study exceptionally fast reactions.

**Figure 4.** NMR spectrum for [Cu^I([15]aneS₃bpy)]⁺ in acetonitrile at ambient temperature, $\mu = 0.10$ M (ClO₄⁻).

check on the value of the self-exchange rate constant for [Cu^{II}/([15]aneS₃bpy)]^{2+/+} was conducted using NMR line-broadening measurements in deuterated acetonitrile at 25 °C. Small amounts of Cu^{II} were added to a stock Cu^IL solution, and the line widths of the selected peaks were measured. The ionic strengths of the solutions were calculated from the known concentrations of the constituent species and corrected to 0.10 M as previously described.²⁶ The data were then plotted in the form:²⁶

$$W_{DP}Q\pi = W_DQ\pi + k_{11}[Cu^{II}L] \quad (6)$$

In this expression, W_{DP} is the peak width at half-height of the selected singlet proton resonance peak for a solution containing both the diamagnetic (Cu^IL) and paramagnetic (Cu^{II}L) species, W_D is the corresponding value for a solution containing only the diamagnetic species, and Q (=1.97) is a factor used to correct the extent of outer-sphere complex formation at the specific ionic strength used to a value of $\mu = 0.10$ M.²⁶

Preliminary NMR line-broadening measurements, based on the line width of the 7.6 ppm peak, yielded $k_{11} = (2.2 \pm 0.1) \times 10^5 M^{-1} s^{-1}$ for 25 °C, corrected to $\mu = 0.10$ M.²⁶ A more carefully prepared series of solutions run under similar conditions yielded $k_{11} = (4.2 \pm 0.6) \times 10^5 M^{-1} s^{-1}$ based on the 7.6 ppm peak width and $(4.0 \pm 0.4) \times 10^5 M^{-1} s^{-1}$ based on the peak at 4.2 ppm. (Experimental data for the latter series are available as Supporting Information.)

Structural Determinations. In conjunction with the current investigation, we have determined the crystal structures for the perchlorate salts of both the oxidized and reduced complexes: [Cu^{II}([15]aneS₃bpy)](ClO₄)₂ and [Cu^I([15]aneS₃bpy)](ClO₄). In both complexes the copper atom is coordinated to all five donor atoms, in agreement with the NMR spectrum. Crystallographic data are listed in Table 3. The bond lengths and bond angles of primary interest for both structures are presented in Table 4. Figure 5 shows the superimposed ORTEP views of the [Cu^{II}([15]aneS₃bpy)]²⁺ and [Cu^I([15]aneS₃bpy)]⁺ cationic units. In both cases, the perchlorate oxygens are more than 4 Å away from the copper atom.

Theoretical Calculations. Previous attempts within our laboratory to make meaningful theoretical calculations regarding

Table 3. Crystal Parameters and Experimental Data for X-ray Diffraction Measurements on the Copper(II) and Copper(I) Complexes Formed with [15]aneS₃bpy^a

parameter	[Cu ^{II} ([15]aneS ₃ bpy)](ClO ₄) ₂	[Cu ^I ([15]aneS ₃ bpy)]ClO ₄
emp. form.	CuC ₁₆ H ₁₈ S ₃ Cl ₂ O ₈	CuC ₁₆ H ₁₈ S ₃ ClO ₄
fw	596.94	479.49
space group	C ₂ /c	C ₂ /c
a, Å	38.152(13)	24.0998(11)
b, Å	5.4157(15)	14.1272(6)
c, Å	20.548(7)	12.6599(5)
α, deg	90	90
β, deg	98.457(9)	120.609(2)
γ, deg	90	90
V, Å ³	4199(2)	3709(3)
Z	8	8
T, K	295(2)	100(2)
ρ _{calcd} , g cm ⁻³	1.888	1.782
μ, mm ⁻¹	1.643	1.686
R(F), I > 2σ ^b	0.0694	0.0461
R _w (F ²), I > 2σ ^c	0.1672	0.1231

^a λ = 0.71703 Å. ^b R(F) = Σ|F_o| - |F_c|/Σ|F_o| for 2σ(I) reflections. ^c R_w(F²) = [Σw(F_o² - F_c²)²/Σw(F_o²)²]^{1/2} for 2σ(I) reflections.

the energy barriers associated with electron transfer in Cu^{II/I} systems had been relatively qualitative, being limited both by the low level of theory used and the difficulty of treating the impact of bond formation/rupture during the electron-transfer process. The fact that the [Cu^{II/I}([15]aneS₃bpy)]^{2+/+} self-exchange reaction occurs without significant changes in coordination geometry suggested that more sophisticated theoretical calculations might be profitable.

Electronic structure calculations were computed by using the TPSS meta-GGA density functional⁴⁵ and a basis set of the quality recommended by Solomon and co-workers.¹⁷ It was recently shown that meta-GGA functionals are well suited for organometallic complexes and generally outperform standard GGA and hybrid functionals.⁶² The C₁ and C_s geometries were optimized for both [Cu^I([15]aneS₃bpy)]⁺ and [Cu^{II}([15]aneS₃bpy)]²⁺ complexes to produce four different optimized structures. The minimized gas-phase C₁ and C_s structures for [Cu^I([15]aneS₃bpy)]⁺ and [Cu^{II}([15]aneS₃bpy)]²⁺, respectively, are in excellent agreement with the resolved crystal structures. It is interesting to note that, when the ligand conformation goes from asymmetric (C₁) to symmetric (C_s), the Cu–S(2) gas-phase bond shortens by 0.06 and 0.02 Å for oxidation states I and II, respectively. As the oxidation state goes from I to II for a given ligand conformation, the Cu–S(2) bond always lengthens by ~0.2 Å, while the other four coordinate bonds contract by ~0.1 Å. This trend is seen in both the computed gas-phase structures and the crystal structures. The electronic energies of the optimized C₁ and C_s geometries for both oxidation states are presented in Table 6. With an energy difference of less than 6 kJ mol⁻¹, both the C₁ and C_s complexes are readily accessible for each oxidation state at room temperature.

While it is not possible to model directly the Cu^{II/I}L/Cu^IL redox reaction energetics due to the complications of properly representing a solvated electron, it is possible to investigate those parts of the reaction path not involving the electron-transfer step itself. In order for the outer-sphere self-exchange electron transfer (eq 1) to occur, the energy of the system containing two Cu centers, denoted *CuL + CuL, with the redox active

electron localized on *CuL, must equal the system's energy with the electron localized on CuL. As a result of the C_s symmetry of the self-exchange system's potential energy surface, in the absence of a perturbing field, this energetic coincidence will occur when *both* oxidation states obtain the coincidence geometry, q_c. It is important to note that identical coincidence geometries for both oxidation states is *not* a requirement for electron transfer but, rather, a manifestation of the underlying particle indistinguishability in self-exchange reactions. Assigning a diabatic potential energy surface to the reactants, q₁, and products, q₂, we arrive at the standard Marcus two-state energy diagram for a symmetric (ΔG° = 0) electron-transfer reaction in Figure 6a.

To probe the energetics associated with merging the two oxidation-state geometries toward q_c, we followed the four-point method of Nelsen et al.⁶³ employing a complete set of redundant internal coordinates. Energies were calculated at seven equidistant points linearly interpolated between the Cu^{II}L and Cu^IL ground-state geometries to determine the electronic component of ΔG* for both the C₁ and C_s surfaces. Since two surfaces are available and energetically accessible for the [15]aneS₃bpy complexes, transition states (TSs) connecting the C₁ and C_s ground states were located for both oxidation states (see Table 6). Although both surfaces are accessible at room temperature, the Cu^IL barrier for C₁ to C_s interconversion is 3 kJ mol⁻¹ lower than the Cu^{II}L barrier.

For comparative purposes, the same optimization and redox-reaction path approaches were applied to the five-coordinate invariant Cu^{II/I} systems involving the acyclic ligands previously reported by Stanbury and co-workers, designated as (py)₂DAP,²¹ (imidH)₂DAP,^{21,22} (5-Meimid)₂DAP,²³ and (imidR)₂DAP,²¹ for which the results are listed in Table 5.

Discussion

For all six cross-reactions studied in this work, the calculated electron self-exchange rate constants are included in Table 2 as logarithmic k₁₁ values. It will be noted that all such values are within an order of magnitude of the corresponding values obtained from NMR line-broadening measurements. This represents an acceptable level of agreement, considering the large number of variables involved in the calculations and the fact that any errors in the experimental k₁₂ or k₂₁ values become squared when calculating k₁₁ (eq 5).⁶ From the combined self-exchange and cross-reaction kinetic data, we conclude that k₁₁ = 1 × 10⁵ M⁻¹ s⁻¹ for the [Cu^{II/I}([15]aneS₃bpy)]^{2+/+} system.

In several Cu^{II/I}L systems previously studied, the k₁₁ values calculated from oxidation reactions differed from those calculated from reductions.^{29,39,60,65–72} This phenomenon has been

- (63) Nelsen, S. F.; Blackstock, S. C.; Kim, Y. *J. Am. Chem. Soc.* **1987**, *109*, 677–682.
 (64) The calculated geometries at the sequential points are based on taking the differences in the bond lengths and bond angles between the ground-state C₁ geometry of Cu^IL and the ground-state C_s geometry of Cu^{II}L and altering each length and angle by one-eighth of these differences for each sequential point.
 (65) Ambundo, E. A.; Yu, Q.; Ochrymowycz, L. A.; Rorabacher, D. B. *Inorg. Chem.* **2003**, *42*, 5267–5273.
 (66) Meagher, N. E.; Juntunen, K. L.; Heeg, M. J.; Salhi, C. A.; Dunn, B. C.; Ochrymowycz, L. A.; Rorabacher, D. B. *Inorg. Chem.* **1994**, *33*, 670–679.
 (67) Salhi, C. A.; Yu, Q.; Heeg, M. J.; Villeneuve, N. M.; Juntunen, K. L.; Schroeder, R. R.; Ochrymowycz, L. A.; Rorabacher, D. B. *Inorg. Chem.* **1995**, *34*, 6053–6064.
 (68) Wijetunge, P.; Kulatililke, C. P.; Dressel, L. T.; Heeg, M. J.; Ochrymowycz, L. A.; Rorabacher, D. B. *Inorg. Chem.* **2000**, *39*, 2897–2905.

(62) Schultz, N. E.; Zhao, Y.; Truhlar, D. G. *J. Phys. Chem. A* **2005**, *109*, 11127–11143.

Table 4. Average Bond Distances and Bond Angles in the Cationic Units of $[\text{Cu}^{\text{II}}([\text{15}]\text{aneS}_3\text{bpy})](\text{ClO}_4)_2$ and $[\text{Cu}^{\text{I}}([\text{15}]\text{aneS}_3\text{bpy})]\text{ClO}_4$

bond distance/angle	$[\text{Cu}^{\text{II}}([\text{15}]\text{aneS}_3\text{bpy})](\text{ClO}_4)_2$	$\text{Cu}^{\text{I}}([\text{15}]\text{aneS}_3\text{bpy})\text{ClO}_4$
Cu–S(1), Å	2.300(3)	2.4226(10)
Cu–S(2), Å	2.475(2)	2.3219(10)
Cu–S(3), Å	2.314(2)	2.3881(9)
Cu–N(1), Å	1.954(7)	2.136(3)
Cu–N(2), Å	1.953(7)	2.141(3)
S(1)–Cu–S(2), deg	90.91(8)	91.92(4)
S(2)–Cu–S(3), deg	90.69(8)	93.36(3)
S(2)–Cu–N(1), deg	99.3(2)	105.33(7)
S(2)–Cu–N(2), deg	98.9(2)	113.00(8)
S(1)–Cu–S(3), deg	105.26(9)	115.95(4)
S(1)–Cu–N(2), deg	85.9(2)	81.10(8)
S(1)–Cu–N(1), deg	165.2(2)	154.76(8)
S(3)–Cu–N(1), deg	85.5(2)	81.87(8)
S(3)–Cu–N(2), deg	165.2(2)	148.70(8)
N(1)–Cu–N(2), deg	81.9(3)	75.29(11)
Cu displacement, Å ^a	+ 0.168(3)	+ 0.369(1)

^a Displacement of the Cu atom from the S_2N_2 plane. The positive values represent displacement of the Cu toward the axial S donor atom.

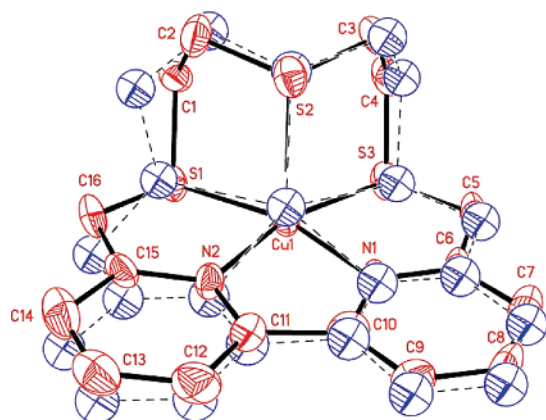


Figure 5. Superimposed ORTEP drawings of the cationic unit in the crystal structure of the oxidized (red) and reduced (blue) complex for $[\text{Cu}^{\text{II/I}}([\text{15}]\text{aneS}_3\text{bpy})]^{2+/+}$ showing the atom numbering scheme. The most notable structural change involves a “puckering” of the C1 and C2 carbon atoms on going from $\text{Cu}^{\text{II}}\text{L}$ to $\text{Cu}^{\text{I}}\text{L}$. Ellipsoids represent 50% probability. Hydrogen atoms have been omitted for clarity.

attributed to ligand conformational changes occurring in a sequential, rather than a concerted, manner with the electron-transfer step. Since the two processes can occur in either order, two competing mechanistic pathways are accessible, one of which involves a metastable $\text{Cu}^{\text{II}}\text{L}$ species (Q) and the other a metastable $\text{Cu}^{\text{I}}\text{L}$ analogue (P) as illustrated in Scheme 1. For most of the studies conducted in our laboratory in which both pathways have been accessed, the more favored pathway has been the one designated as Pathway A in Scheme 1.^{29,39,66–69} This implies that the $\text{Cu}^{\text{I}}\text{L}$ metastable intermediate, $\text{Cu}^{\text{I}}\text{L}(\text{P})$, is relatively more stable than the corresponding $\text{Cu}^{\text{II}}\text{L}$ intermediate, $\text{Cu}^{\text{II}}\text{L}(\text{Q})$, in those systems. However, for complexes with some tripodal ligands⁶⁵ and for the bis complexes with some substituted derivatives of bipyridyl ligands studied by Takagi and co-workers^{71,72} Pathway B appears to be more favorable.

In the current system, the same k_{11} value was obtained for both oxidation and reduction within experimental error. Under these circumstances, the data obtained for both the oxidation

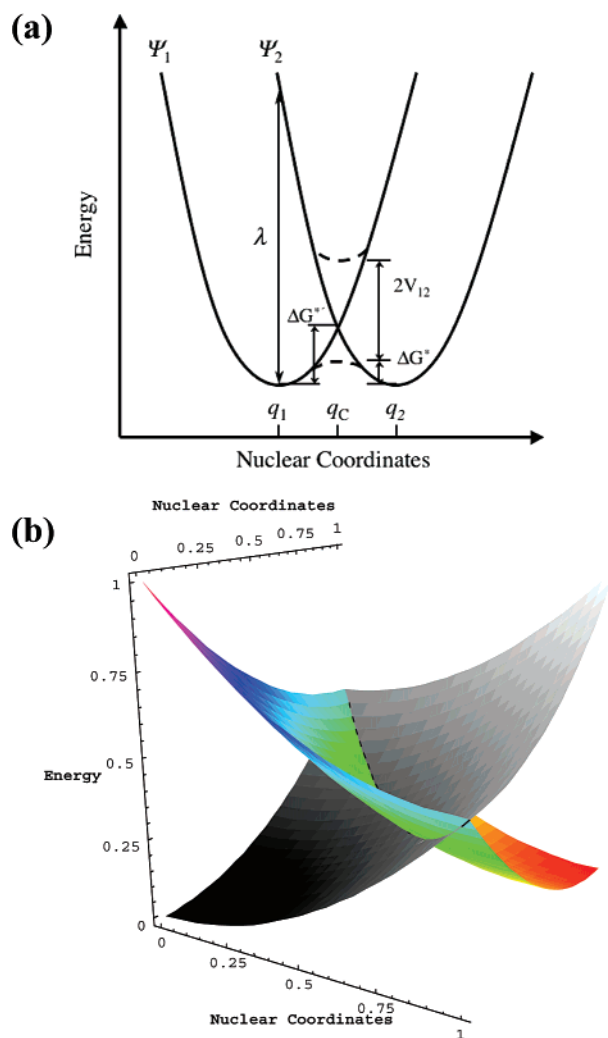


Figure 6. Two-state potential energy diagram in (a) two- and (b) three-dimensions. The energy at the coincidence geometry, q_c in (a), is the diabatic activation energy, $\Delta G^{*'}$, λ is the reorganization energy, and ΔG^* is the activation energy. The grayscale surface in (b) is Ψ_1 and the colored surface is Ψ_2 . The intersection of Ψ_1 and Ψ_2 is the seam of all possible coincidence geometries. The self-exchange ground states, q_1 and q_2 in part (a), correspond to points $\{0,0,0\}$ and $\{1,1,0\}$ in part (b), respectively. At $\{0,0,1\}$ both Cu centers are in the $\text{Cu}^{\text{I}}\text{L}$ ground-state geometry, while at $\{1,1,1\}$ both centers have adopted the ground-state geometry of $\text{Cu}^{\text{II}}\text{L}$.

and reduction reactions are presumed to be proceeding by the same reaction pathway, implying that the ground-state species

(69) Yu, Q.; Salhi, C. A.; Ambundo, E. A.; Heeg, M. J.; Ochrymowycz, L. A.; Rorabacher, D. B. *J. Am. Chem. Soc.* **2001**, *123*, 5720–5729.

(70) Ambundo, E. A.; Ochrymowycz, L. A.; Rorabacher, D. B. *Inorg. Chem.* **2001**, *40*, 5133–5138.

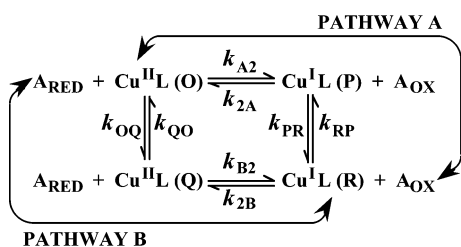
(71) Koshino, N.; Kuchiyama, Y.; Funahashi, S.; Takagi, H. D. *Can. J. Chem.* **1999**, *77*, 1498–1507.

(72) Koshino, N.; Kuchiyama, Y.; Ozaki, H.; Funahashi, S.; Takagi, H. D. *Inorg. Chem.* **1999**, *38*, 3352–3360.

Table 5. Comparative Self-Exchange Rate Constants for Coordination-Invariant Quinque- and Quadridentate Copper(II/I) Systems Plus Rapidly Reacting Systems with Variable Coordination at 25 °C, $\mu = 0.10$ M

coordinated ligand	$\log k_{11}$ ($M^{-1} s^{-1}$) ^a	Calcd ΔE^{\ddagger} ($kJ mol^{-1}$) ^c
Coordination Invariant: Five-Coordinate		
[15]aneS ₃ bpy	4.5– 5.6 ^b	12.6 (15.1) ^c
(5-Meimid) ₂ DAP	4.5 ^d	16.5
(imidR) ₂ DAP	3.5 ^e	15.3
(imidH) ₂ DAP	3.2– 4.1 ^{e,f}	16.5
(py) ₂ DAP	2.5–3.2 ^e	18.1
Coordination Invariant: Four-Coordinate		
HB(3,5- <i>i</i> Pr ₂ py) ₃ + C ₆ F ₅ S ⁻	5.5 (?) ^g	
bis-bimdpk	4.3 ^h	
bis-(dpym ⁻)	3.8 ⁱ	
W ₁₂ O ₄₀ ⁸⁻	0.4 ⁱ	
bis-bib	– (1.6–0.3) ^k	
bite	– (1.9–1.2) ^l	
Variable Coordination: Five-Coordinate → Four-Coordinate		
oxathiane-[12]aneS ₄	5.6– 5.9 ^m	
TAAB	5.7 ⁿ	
[15]aneS ₅	4.9–5.5 (5.0) ^{o,p}	
[15]aneNS ₄	4.4– 5.1 ^q	

^a Values in boldface were determined by NMR line-broadening; all other values are based on application of the Marcus relationship to cross-reactions. ^b This work. ^c ΔE^{\ddagger} values represent gas-phase calculations except for the parenthetical value for [15]aneS₃bpy which includes the contributions of a solvent continuum in acetonitrile (see text). ^d Reference 23. ^e Reference 21. ^f Reference 22. ^g Reference 73; NMR line-broadening data were nonlinear and were extrapolated from a very low temperature (see text). ^h Reference 25. ⁱ Reference 24. ^j Lappin, A. G.; Peacock, R. D. *Inorg. Chim. Acta* **1980**, *46*, L71–L72. ^k Reference 19. ^l Reference 20. ^m Reference 28. ⁿ Reference 30. ^o Reference 26. ^p Reference 60. ^q Reference 27.

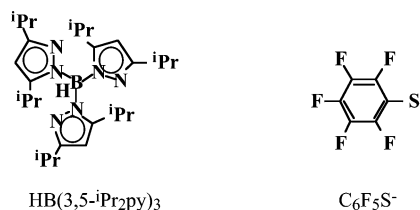
Scheme 1

and the metastable intermediate for the dominant pathway are in rapid equilibrium relative to the rate of the electron-transfer step. Under these circumstances it is impossible to determine which pathway is involved, nor is it possible to distinguish between a sequential and a concerted pathway. It is interesting to note, however, that the same pattern of behavior has been observed with nearly all other Cu^{II/I} systems studied to date in which a quinque- and quadridentate ligand is coordinated to the copper atom—that is, all such systems have generated a single k_{11} value—regardless of whether the system remains five-coordinate or changes to four-coordinate upon reduction.^{21–23,26,27}

Previous studies on Cu^{II/I}L systems maintaining five-coordinate geometries in both oxidation states, as reported by Stanbury, Wilson, and co-workers,^{21–23} are included in Table 5. These closely related acyclic ligands—(py)₂DAP, (imidH)₂DAP, (imidR)₂DAP, and (5-Meimid)₂DAP—involve five imine nitrogen donor atoms (see Figure 1). Although little cross-reaction rate data are available for these systems, the reported k_{11} values appear to lie within the range of 2×10^3 to $3 \times 10^4 M^{-1} s^{-1}$ as determined from NMR line-broadening studies (Table 5), that is, they are 1–2 orders of magnitude smaller than the values obtained from NMR measurements on the [Cu^{II/I}-(15]aneS₃bpy)]^{2+/+} complex in this work. Similar k_{11} values

have been reported for the Cu^{II/I} complexes with the sterically hindered bidentate ligands designated as dpym⁻ and bimdpk (Figure 1) which have been shown to remain four-coordinate in both oxidation states.^{24,25} By contrast, the k_{11} values reported by Stanbury and co-workers for [Cu^{II/I}(bib)₂]^{2+/+}¹⁹ and [Cu^{II/I}(bite)]^{2+/+}²⁰ both of which are presumed to remain four-coordinate upon electron transfer, are remarkably small, an observation that has not yet been satisfactorily explained.

Recently, Fujisawa and co-workers⁷³ reported the first electron-transfer kinetic study on a Cu^{II/I} complex containing a Cu–S(mercaptide) bond which maintains four-coordinate in both oxidation states. The complex involves a coordinated tripodal ligand, hydrotris(3,5-diisopropyl-1-pyrazolyl)borate ligand (HB(3,5-*i*Prpy)₃ = L), plus a pentafluorobenzenethiolate ligand (C₆F₅S⁻), the latter of which provides a coordinated mercaptide sulfur donor atom. On the basis of NMR line-broadening measurements in deuterated acetone at –20 to –60 °C, they reported a value of $k_{11} = 3.14 \times 10^5 M^{-1} s^{-1}$ (corrected to 25 °C).



The Supporting Information provided with Fujisawa's article reveals that the experimental line width plots were so badly curved that the asymptotic slopes obtained from the lowest and highest Cu^{II} concentrations differ by an order of magnitude at each temperature studied. Thus, not only are the individual k_{11} values for each experimental temperature ill-defined, but the curvature also leaves some doubt as to whether the data actually represent line-broadening due to electron exchange. At the very least, the uncertainty associated with the line width trend at each temperature, plus the uncertainty inherent in extrapolating the low-temperature data to +25 °C, suggests that their self-exchange rate constant is, at best, known only to the nearest order of magnitude, that is, $k_{11} \approx 10^5 M^{-1} s^{-1}$. If the latter value has validity, it would appear to corroborate Solomon and Ryde's conclusions regarding the impact of the electronic effects induced by the copper–mercaptide sulfur bond upon electron-transfer kinetics.^{17,18} However, it leaves open the question as to whether similar rapid electron-transfer kinetics can be observed in coordination-invariant Cu^{II/I} systems based solely on the type of geometric entatic state originally envisioned by Vallee and Williams.

To understand our theoretical results, we begin by defining the distortion energy for a particular set of nuclear coordinates as the electronic energy at that geometry minus the electronic energy of the ground-state geometry for a particular oxidation state. In terms of distortion energies, self-exchange electron transfer occurs when the total distortion energy of the Cu^{II}L +

(73) Fujisawa, K.; Fujita, K.; Takahashi, T.; Kitajima, N.; Moro-oka, Y.; Matsunaga, Y.; Miyashita, Y.; Okamoto, K. *Inorg. Chem. Commun.* **2004**, *7*, 1188–1190 (the experimental linewidth values are provided as Supporting Information). Additional structural and spectroscopic information on the [Cu^{II/I}(HB(3,5-*i*Prpy)₃(SC₆F₅)] system is reported in: (a) Kitajima, N.; Fujisawa, K.; Tanaka, M.; Moro-oka, Y. *J. Am. Chem. Soc.* **1992**, *114*, 9232–9233. (b) Matsunaga, Y.; Fujisawa, K.; Ibi, N.; Miyashita, Y.; Okamoto, K. *Inorg. Chem.* **2005**, *44*, 325–335.

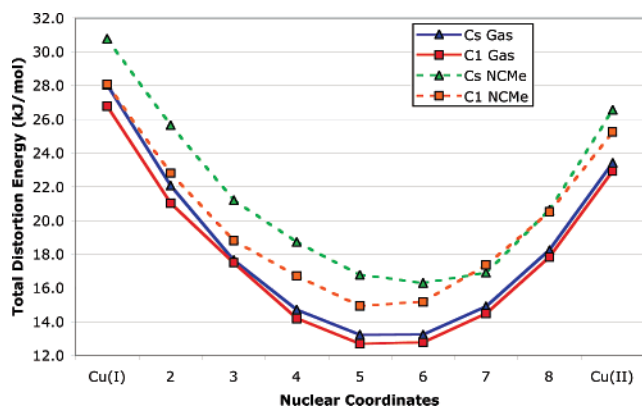


Figure 7. Total distortion energy for the $[\text{Cu}^{\text{II}}]([15]\text{aneS}_3\text{bpy}) + [\text{Cu}^{\text{I}}]([15]\text{aneS}_3\text{bpy})$ self-exchange system when both species adopt the same geometry. Point 1 represents the electronic reorganization energy required to distort $\text{Cu}^{\text{II}}\text{L}$ to the C_1 ground-state geometry of $\text{Cu}^{\text{I}}\text{L}$ for a given symmetry and phase, while point 9 is the electronic reorganization energy required to distort $\text{Cu}^{\text{I}}\text{L}$ to the C_s ground-state geometry of $\text{Cu}^{\text{II}}\text{L}$ for that same symmetry and phase. Points 2–8 are equidistant configurations as the molecular geometry of the $\text{Cu}^{\text{I}}\text{L}$ and $\text{Cu}^{\text{II}}\text{L}$ species are stepped from the $\text{Cu}^{\text{I}}\text{L}$ ground state to the $\text{Cu}^{\text{II}}\text{L}$ ground state. The solid curves represent gas-phase species, while the dashed curves include a dielectric continuum approximating the acetonitrile solvent shell. The minimum in the total distortion energy provides an upper boundary to $E^{*'}$.

$\text{Cu}^{\text{I}}\text{L}$ system is minimized. Since the coincidence geometry is the same for both oxidation states in self-exchange reactions, it is very tempting to interpret the intersection of the $\text{Cu}^{\text{II}}\text{L}$ and $\text{Cu}^{\text{I}}\text{L}$ distortion energy curves as the point of electron transfer, but that ignores the different definitions of zero energy for each curve. Using the $\text{Cu}^{\text{II}}\text{L}$ and $\text{Cu}^{\text{I}}\text{L}$ ground-state geometries plus the seven interpolated structures, the total distortion energy along a linear path from reactants to products is plotted for the C_1 and C_s surfaces in Figure 7. After fitting polynomials to these data, the minimum distortion energy and corresponding geometry provide an upper boundary to the electronic component of the diabatic activation energy, $\Delta E^{*'}$, and a reasonable approximation to q_c , respectively. (See Supporting Information for individual data and fits.) Location of the true self-exchange $\Delta E^{*'}$ requires optimization along the $3N - 7$ seam of intersection, where N is the number of nuclei in CuL .

In Figure 7, point 1 denotes the energy required to distort the ground states of $\text{Cu}^{\text{II}}\text{L}$ and $\text{Cu}^{\text{I}}\text{L}$ into the ground-state geometry of $\text{Cu}^{\text{I}}\text{L}$. Since $\text{Cu}^{\text{I}}\text{L}$ is already in its ground state, the energy at point 1 (28.0 and 26.8 kJ mol^{-1} for C_s and C_1 , respectively) is equal to the internal electronic reorganization energy, λ_i , for $\text{Cu}^{\text{II}}\text{L}$. Likewise, point 9 gives λ_i (23.4 and 22.9 kJ mol^{-1} for C_s and C_1 , respectively) for $\text{Cu}^{\text{I}}\text{L}$ and indicates that $\text{Cu}^{\text{I}}\text{L}$ is more easily distorted than $\text{Cu}^{\text{II}}\text{L}$. Since the corresponding q_c values (5.46 and 5.49 for C_s and C_1 , respectively)—corresponding to the abscissa scale in Figure 7) are greater than five, the coincidence geometry is slightly closer to the ground-state geometry for $\text{Cu}^{\text{II}}\text{L}$.

It should be re-emphasized that the calculations outlined above represent a concerted mechanism on a surface of uniform symmetry, which does not presume the existence of metastable intermediates of the type designated in Scheme 1. Since each oxidation state has different distortion energies for a given geometry, even concerted mechanisms will rarely have coincidence geometries whose bond lengths and angles are exactly halfway between those found in the ground state for the two reacting partners. Nonetheless, our approach does provide insight

Table 6. Calculated Electronic Energy for $[\text{Cu}^{\text{I}}]([15]\text{aneS}_3\text{bpy})$ and $[\text{Cu}^{\text{II}}]([15]\text{aneS}_3\text{bpy})$ Complexes with Values Relative to the Ground State for Each Oxidation State

molecule	symmetry	relative electronic energy, kJ mol^{-1}	
		gaseous state	with solvation shell
$\text{Cu}^{\text{I}}\text{L}$	C_1	0.00	0.00
$\text{Cu}^{\text{I}}\text{L}$	C_s	5.41	3.66
$\text{Cu}^{\text{I}}\text{L}^*$ (TS) ^a	C_1	18.14	18.03
$\text{Cu}^{\text{II}}\text{L}$	C_1	0.00	0.50
$\text{Cu}^{\text{II}}\text{L}$	C_s	2.63	0.00
$\text{Cu}^{\text{II}}\text{L}^*$ (TS) ^a	C_1	21.49	20.49

^a Calculated transition state.

into the relative energetics involved in achieving the common coincidence geometry that must exist for self-exchange electron transfer to occur between $\text{Cu}^{\text{I}}\text{L}$ and $\text{Cu}^{\text{II}}\text{L}$.

For comparative purposes, the computed gas-phase, electronic components of the diabatic activation energy, $\Delta E^{*'}$, have been calculated for the other five-coordinate invariant systems previously studied by Stanbury and co-workers. The results are summarized in Table 5. Once again, these calculations are based on the presumption of a concerted mechanism. It is noted that the acyclic ligands containing imidazole groups bound to Cu have activation energies clustered around 16 kJ mol^{-1} . Although the $(\text{py})_2\text{DAP}$ ligand has the same conformational flexibility as the imidazole-containing ligands, the activation barrier is ~ 2 kJ mol^{-1} larger. This system has been reported to react more slowly than its imidazole analogues. Table 5 also reveals that, among the investigated five-coordinate ligand systems, the smallest diabatic activation barrier is seen for the $[\text{Cu}^{\text{II}}]([15]\text{aneS}_3\text{bpy})^{2+/+}$ system, which has the least ligand flexibility and exhibits the largest k_{11} value. The rough parallel between the calculated $\Delta E^{*'}$ values and the experimentally obtained k_{11} values for these five five-coordinate invariant systems tends to support the validity of our computational approach.

The foregoing calculations omit any contribution of the outer-sphere solvent reorganization that may, in fact, be very significant.⁷⁴ In an attempt to assess the influence of the surrounding acetonitrile solvent shell upon the solvent reorganization energy, we repeated the calculations for the $[15]\text{aneS}_3\text{bpy}$ system employing the integral equation formalism of the polarizable continuum model (IEF-PCM) with a dielectric value of 36.64.⁷⁵ For both the C_1 and C_s surfaces, the relative energy difference of the two ground-state species decreased slightly for each oxidation state as shown in Table 6. Interestingly, the relative energies of the C_1 and C_s surfaces reverse so that the C_s geometry for $[\text{Cu}^{\text{II}}]([15]\text{aneS}_3\text{bpy})^{2+}$, which was observed in the crystal structure, is now the ground state. These new structures were used to generate solvated total distortion curves for Figure 7 in the same manner as described above. It should be noted that the geometries plotted on the abscissa differ for each phase and geometry. Although the transition states for both oxidation states have lower energies in solution, the Cu^{I} barrier for C_1 -to- C_s interconversion is still 3 kJ mol^{-1} smaller than the Cu^{II} barrier. In the gas-phase, $\Delta E^{*'}$ is 12.60 and 13.01 kJ mol^{-1}

(74) Comba, P.; Kerscher, M.; Roodt, A. *Eur. J. Inorg. Chem.* **2004**, 4640–4645.

(75) (a) Cancès, E.; Mennucci, B.; Tomasi, J. *J. Chem. Phys.* **1997**, *107*, 3032–3041. (b) Mennucci, B.; Tomasi, J. *J. Chem. Phys.* **1997**, *106*, 5151–5158. (c) Mennucci, B.; Cancès, E.; Tomasi, J. *J. Phys. Chem. B* **1997**, *101*, 10506–10517. (d) Tomasi, J.; Mennucci, B.; Cancès, E. *J. Mol. Struct. (THEOCHEM)* **1999**, *464*, 211–226.

for the C_1 and C_s surfaces, respectively, indicating that the C_1 pathway is only slightly more favorable. With the inclusion of continuum solvation effects, the corresponding activation energies are 15.08 and 16.12 kJ mol⁻¹ for the C_1 and C_s surfaces, respectively.

Conclusion

Comba has provided an extensive analysis of the entatic state concept, including attempts made to generate Cu^{II/I}L systems which provide physical constraints intended to generate geometric entatic states in accordance with the original concept espoused by Vallee and Williams.⁷⁶ Of the coordination-invariant Cu^{II/I}L systems for which electron self-exchange rate constants have been reported to date, the [Cu^{II/I}([15]aneS₃bpy)]^{2+/+} system represents the most convincing example of a redox couple exhibiting rapid electron-transfer kinetics brought about by a geometrically constrained entatic state. If the redox reaction proceeds through a metastable intermediate, thereby changing molecular symmetry before or after the electron transfer, then Pathway A is the preferred mechanism due to the lower C_1 to C_s barrier for Cu^IL in both solution and gas phases. However,

neither the theoretical calculations nor the experimental kinetic data allow us to rule out the possibility of a concerted mechanism for the [Cu^{II/I}([15]aneS₃bpy)]^{2+/+} system in acetonitrile. The relatively small energy barrier associated with the geometric change (12.6 kJ mol⁻¹ for the system in a vacuum; 15.1 kJ mol⁻¹ when including a solvent continuum) appears to confirm the hypothesis that the overall reorganizational energy barrier for electron transfer in geometrically constrained Cu^{II/I} systems can be successfully minimized by appropriate ligand constraints.

Acknowledgment. This work was supported by the National Science Foundation under Grant CHE-0211696. We thank Professor John F. Endicott for helpful discussions and Dr. Lew Hryhorczuk of Wayne State University's Central Instrument Facility for assistance in generating electrospray mass spectral data.

Supporting Information Available: Experimental rate constant data for cross-reactions, NMR line-broadening data, and tables of DFT calculations. This material is available free of charge via the Internet at <http://pubs.acs.org>.

(76) Comba, P. *Coord. Chem. Rev.* **2000**, *200*, 217–245.

JA068960U